PERGAMON

International Journal of Heat and Mass Transfer 45 (2002) 3111–3123

International Journal of HEAT and MASS TRANSFER

www.elsevier.com/locate/ijhmt

Interfacial area transport equation: model development and benchmark experiments

M. Ishii [a], S. Kim [a,*], J. Uhle [b]

[a] *Thermal-Hydraulics and Reactor Safety Laboratory, School of Nuclear Engineering, Purdue University, West Lafayette, IN 47907-1290, USA*

[b] *T10K8 US Nuclear Regulatory Commission, 11545 Rockville Pike, Rockville, MD 20852, USA*

Received 16 July 2001; received in revised form 8 January 2002

Abstract

The interfacial area transport equation dynamically models two-phase flow regime transitions and predicts continuous changes of the interfacial area concentration along the flow field. It replaces the flow regime-dependent correlations for the interfacial area concentration in thermal-hydraulic system analysis. In the present study, detailed formulation of the interfacial area transport equation is presented along with its evaluation results based on the detailed benchmark experiments. In view of model evaluation, the equation is simplified into one-dimensional steady state one-group interfacial area transport equation. The prediction made by model agrees well with the experimental data obtained in round pipes of various diameters. The framework for the two-group transport equation and the necessary constitutive relations are also presented in view of bubble transport of various sizes and shapes.

Keywords: Interfacial area transport equation; Number transport; Void fraction transport; One-group transport; Two-group transport; Two-fluid model

1. Introduction

In predicting the thermal-hydraulic behavior of the two-phase flow, the interfacial structure is one of the most important parameters, since all the transfers of mass, momentum and energy between phases occur at the interface. In the two-fluid model [1–3], these interfacial terms are represented in the conservation equations of mass, momentum and energy, which are solved for each phase. As a result, the two-fluid model has the capacity to predict detailed phasic interactions, which is not possible with more simplified mixture models. However, for the two-fluid model to be valid, the interfacial interaction terms must be accurate, since without them, the two phases are virtually independent. Simply, the interaction terms determine the degree of coupling between the phases. In view of practical applications, Ishii and Mishima [4,5] simplified the two-fluid model equations of mass, momentum and energy as

$$\frac{\partial \alpha_k \rho_k}{\partial t} + \nabla \cdot (\alpha_k \rho_k v_k) = \Gamma_k; \tag{1}$$

$$\frac{\partial \alpha_k \rho_k v_k}{\partial t} + \nabla \cdot (\alpha_k \rho_k v_k v_k) = -\alpha_k \nabla p_k + \nabla \cdot \alpha_k (\bar{\bar{\tau}} + \tau_k^t) + \alpha_k \rho_k g + v_{ki} \Gamma_k + M_{ki} - \nabla \alpha_k \cdot \tau_i; \tag{2}$$

$$\frac{\partial \alpha_k \rho_k H_k}{\partial t} + \nabla \cdot (\alpha_k \rho_k H_k v_k) = -\nabla \cdot \alpha_k (\overline{\overline{q_k}} + q_k^t) + \alpha_k \frac{D_k}{Dt} p_k + H_{ki} \Gamma_k + \frac{q''_{ki}}{L_s} + \phi_k, \tag{3}$$

where Γ_k, M_{ki}, τ_i, q''_{ki} and ϕ_k are the mass generation, generalized interfacial drag, interfacial shear stress, interfacial heat flux and dissipation, respectively. The subscript i denotes the value at the interface. The term L_s

* Corresponding author. Tel.: +1-765-494-5759; fax: +1-765-494-9570.

E-mail address: seungjin@ecn.purdue.edu (S. Kim).

0017-9310/02/$ - see front matter
PII: S0017-9310(02)00041-8

Nomenclature

A_i	average surface area of fluid particles
a_i	interfacial area concentration
B_d	volume of a typical dispersed fluid particle
D_b	bubble diameter
D_{dmax}	maximum distorted bubble limit
D_e	volume equivalent diameter
D_s	surface area equivalent diameter
D_{sm}	bubble Sauter mean diameter
$\boldsymbol{F}_D$	standard drag force
$\boldsymbol{F}_V$	virtual mass force
f	fluid particle number density distribution function per unit mixture and bubble volume
h_{ki}	interfacial heat transfer coefficient
L_s	length scale
M_{ki}	generalized interfacial drag
m_k	mean mass transfer rate
$n(\boldsymbol{x},t)$	total number of particles of all sizes per unit mixture volume
q''_{ki}	interfacial heat flux
R_j	jth particle number source/sink rates per unit mixture volume
S_j	jth particle source/sink rates per unit mixture volume
T_i	temperature at the interface
T_k	bulk temperature
t	time
V	fluid particle volume
$\boldsymbol{v}$	fluid particle velocity
$\boldsymbol{v}_i$	interfacial velocity
$\boldsymbol{v}_{pm}$	average local particle velocity weighted by the particle number

Greek symbols

α	void fraction
η_{ph}	rate of volume generated by nucleation per unit mixture volume
ϕ_j	jth interfacial area source or sink rate
ϕ_k	heat dissipation rate
Γ_k	mass generation rate
μ_m	mixture viscosity
τ_i	interfacial shear stress

Subscripts

f	liquid
g	gas
i	interface
ph	phase change

denotes the length scale at the interface, so that $1/L_s$ has the physical meaning of the interfacial area per unit mixture volume [2]

$$\frac{1}{L_s} = a_i. \tag{4}$$

In Eqs. (1)–(3), the generation of mass per unit volume, the generalized drag force per unit volume and the interfacial energy transfer per unit volume constitute the interfacial transfer terms and are modeled [2,4,5], respectively, as

$$\Gamma_k \equiv a_i m_k; \tag{5}$$

$$M_{id} = \frac{\alpha_d \boldsymbol{F}_D}{B_d} + \frac{\alpha_d \boldsymbol{F}_V}{B_d} + \frac{9}{2}\frac{\alpha_d}{r_d}\sqrt{\frac{\rho_c \mu_m}{\pi}} \times \int_t \frac{D_d}{D\xi}(\boldsymbol{v}_d - \boldsymbol{v}_c)\frac{d\xi}{\sqrt{t-\xi}}; \tag{6}$$

$$\Gamma_k H_{ki} + \frac{q''_{ki}}{L_s} = a_i[m_k H_{ki} + h_{ki}(T_i - T_k)]. \tag{7}$$

In Eqs. (5) and (6), $m_k, \boldsymbol{F}_D, B_d, \boldsymbol{F}_V$, and μ_m are the mean mass transfer rate, standard drag force, volume of a typical dispersed fluid particle, virtual mass force and mixture viscosity, respectively. With the last term in the RHS of Eq. (6) being the Basset force, the interfacial transfer term due to the standard drag can be written in terms of interfacial area concentration [4,5] such that

$$\frac{\alpha_d \boldsymbol{F}_D}{B_d} = -a_i\left[\frac{C_D}{4}\left(\frac{r_{sm}}{r_D}\right)\frac{\rho_c \boldsymbol{v}_r|\boldsymbol{v}_r|}{2}\right]. \tag{8}$$

The interfacial energy transfer term, q''_{ki} can be modeled using the driving force or the potential for an energy transfer. Hence, in Eq. (7), T_i and T_k are the temperature at the interface and the bulk temperature based on the mean enthalpy, and h_{ki} is the interfacial heat transfer coefficient.

As shown in Eqs. (5)–(8), the phasic interaction terms are expressed in terms of interfacial area concentration and the driving force such that

$$(\text{Interfacial transfer term}) \sim a_i \times (\text{Driving force}). \tag{9}$$

Therefore, an accurate closure relation for the interfacial area concentration must be provided in order for the two-fluid model to predict the behavior of two-phase flow.

Traditionally, the effects of interface structure have been analyzed using flow regimes and transition criteria [4–7]. However, this approach does not dynamically represent the changes in interfacial structure. Such an approach, which is currently implemented in most two-fluid thermal-hydraulic system analysis codes, can lead to

instantaneous changes in flow regime. Instantaneous changes in flow regime not only induce non-physical oscillations in system behavior but can also limit the code accuracy. Therefore, improvements in the treatment of interfacial structure and flow regime transition are indispensable in the improvement of the code prediction.

To better represent the effects of interfacial structure and the flow regime transition, the use of the first-order equation to characterize the interfacial area transport has been recommended [4,5]. In view of this, Kocamustafaogullari and Ishii [8] established the foundation of the interfacial area transport equation by employing the population balance approach suggested by Reyes [9]. It was followed by the formulation of the preliminary interfacial area transport equation for the bubbly flow by Wu et al. [10], where the source and sink terms were established through mechanistic modeling of bubble interaction phenomena in the bubbly flow regime. Recently, the model has been improved by Kim [11] by analyzing the experimental data in a wide range of bubbly flow.

2. Interfacial area transport equation

The foundation of the interfacial area transport equation stems from the Boltzmann transport equation, where the equation is expressed as an integro-differential equation of the particle distribution function. Letting $f(V,\boldsymbol{x},\boldsymbol{v},t)$ be the particle number density distribution function per unit mixture and bubble volume, which is assumed to be continuous and specifies the probable number density of fluid particles moving with particle velocity $\boldsymbol{v}$, at a given time t, in the spatial range $\delta\boldsymbol{x}$ about a position $\boldsymbol{x}$, with particle volumes between V and $V+\delta V$, we can write

$$f(V+\delta V,\boldsymbol{x}+\boldsymbol{v}\delta t,\boldsymbol{v}+\boldsymbol{F}\delta t,t+\delta t)\delta\mu - f(V,\boldsymbol{x},\boldsymbol{v},t)\delta\mu = \left[\sum_j S_j + S_{\mathrm{ph}}\right]\delta\mu\delta t, \tag{10}$$

where $\delta\mu$ is a volume element in μ space and $\boldsymbol{F}(V,\boldsymbol{x},\boldsymbol{v},t)$ is the force per unit mass. The S_j and S_{ph} are the particle source/sink rates per unit mixture volume due to jth particle interactions such as break-up or coalescence and the source rate due to phase change, respectively. In Eq. (10), if we assume that the change of particle velocity within the time interval t to $t+\delta t$ is negligible, then the distribution function can be approximated as a function of $f(V,\boldsymbol{x},t)$, and the equation reduces to

$$\frac{\partial f}{\partial t} + \nabla\cdot(f\boldsymbol{v}) + \frac{\partial}{\partial V}\left(f\frac{\mathrm{d}V}{\mathrm{d}t}\right) = \sum_j S_j + S_{\mathrm{ph}}. \tag{11}$$

Eq. (11) is analogous to Boltzmann transport equation for particles whose distribution is specified by the distribution function $f(V,\boldsymbol{x},t)$ with sources and sinks furnished by S_j's.

2.1. Number transport equation

Since the particle transport equation given by (11) is much too detailed to be employed in practice, it should be averaged over all particle sizes for practical application. Therefore, integrating it over the volume of all sizes of particles from $V_{\min}$ to $V_{\max}$, the number transport equation for the fluid particle is obtained as

$$\frac{\partial n}{\partial t} + \nabla\cdot(n\boldsymbol{v}_{\mathrm{pm}}) = \sum_j R_j + R_{\mathrm{ph}}, \tag{12}$$

where

$$n(\boldsymbol{x},t) = \int_{V_{\min}}^{V_{\max}} f(V,\boldsymbol{x},t)\,\mathrm{d}V$$

and

$$R(\boldsymbol{x},t) = \int_{V_{\min}}^{V_{\max}} S(V,\boldsymbol{x},t)\,\mathrm{d}V. \tag{13}$$

Here, $n(\boldsymbol{x},t)$ is the total number of particles of all sizes per unit mixture volume, and $\boldsymbol{v}_{\mathrm{pm}}$ is the average local particle velocity weighted by the particle number defined by

$$\boldsymbol{v}_{\mathrm{pm}}(\boldsymbol{x},t) \equiv \frac{\int_{V_{\min}}^{V_{\max}} f(V,\boldsymbol{x},t)\boldsymbol{v}(V,\boldsymbol{x},t)\,\mathrm{d}V}{\int_{V_{\min}}^{V_{\max}} f(V,\boldsymbol{x},t)\,\mathrm{d}V}. \tag{14}$$

2.2. Void fraction transport equation

The volumetric fraction (or void fraction) transport equation can be obtained in a similar manner. Multiplying Eq. (11) by particle volume V, and integrating it over the volumes of all particles, we obtain

$$\frac{\partial\alpha}{\partial t} + \nabla\cdot(\alpha\boldsymbol{v}_{\mathrm{g}}) + \int_{V_{\min}}^{V_{\max}} V\frac{\partial(f\dot{V})}{\partial V}\,\mathrm{d}V = \int_{V_{\min}}^{V_{\max}}\left[\sum_j S_j V + S_{\mathrm{ph}}V\right]\mathrm{d}V, \tag{15}$$

where $\dot{V}$ denotes $\mathrm{d}V/\mathrm{d}t$, and the void fraction and the average velocity of center of volume of the gas phase are given by

$$\alpha(\boldsymbol{x},t) = \int_{V_{\min}}^{V_{\max}} f(V,\boldsymbol{x},t)V\,\mathrm{d}V, \tag{16}$$

and

$$\boldsymbol{v}_{\mathrm{g}}(\boldsymbol{x},t) \equiv \frac{\int_{V_{\min}}^{V_{\max}} f(V,\boldsymbol{x},t)V\boldsymbol{v}(V,\boldsymbol{x},t)\,\mathrm{d}V}{\int_{V_{\min}}^{V_{\max}} f(V,\boldsymbol{x},t)V\,\mathrm{d}V}, \tag{17}$$

respectively.

Here, in solving the third term in the LHS of Eq. (15), we may assume

$$\frac{\dot{V}}{V} \neq f(V), \tag{18}$$

such that the time rate of change of the particle volume is independent of its volume. Then, the third term in the LHS of Eq. (15) reduces to

$$\int_{V_{\min}}^{V_{\max}} V \frac{\partial(f\dot{V})}{\partial V}\,\mathrm{d}V = -\left(\frac{\dot{V}}{V}\right)\alpha(\boldsymbol{x},t). \tag{19}$$

In Eq. (19), $(\dot{V}/V)$ is the volume source, representing the total rate of change of particle volume V. Hence, recalling that the total mass transfer by evaporation is given by

$$\frac{\mathrm{d}\rho_{\mathrm{g}}V}{\mathrm{d}t} = \frac{(\Gamma_{\mathrm{g}} - \eta_{\mathrm{ph}}\rho_{\mathrm{g}})V}{\alpha}, \tag{20}$$

where Γ_{g} is the total rate of change of mass per unit mixture volume and η_{ph} is the rate of volume generated by nucleation per unit mixture volume, defined by

$$\eta_{\mathrm{ph}} \equiv \int_{V_{\min}}^{V_{\max}} S_{\mathrm{ph}} V\,\mathrm{d}V, \tag{21}$$

we obtain

$$\begin{aligned}\frac{1}{V}\frac{\mathrm{d}V}{\mathrm{d}t} &= \frac{1}{\rho_{\mathrm{g}}}\left[\frac{\Gamma_{\mathrm{g}} - \eta_{\mathrm{ph}}\rho_{\mathrm{g}}}{\alpha} - \frac{\mathrm{d}\rho_{\mathrm{g}}}{\mathrm{d}t}\right]\\ &= \frac{1}{\alpha}\left[\frac{\partial\alpha}{\partial t} + \nabla\cdot\alpha\boldsymbol{v}_{\mathrm{g}} - \eta_{\mathrm{ph}}\right].\end{aligned} \tag{22}$$

Therefore, the void fraction transport equation is given by

$$\begin{aligned}&\frac{\partial\alpha}{\partial t} + \nabla\cdot(\alpha\boldsymbol{v}_{\mathrm{g}}) - \frac{\alpha}{\rho_{\mathrm{g}}}\left[\frac{\Gamma_{\mathrm{g}} - \eta_{\mathrm{ph}}\rho_{\mathrm{g}}}{\alpha} - \frac{\mathrm{d}\rho_{\mathrm{g}}}{\mathrm{d}t}\right]\\ &\quad = \int_{V_{\min}}^{V_{\max}}\left[\sum_j S_j V + S_{\mathrm{ph}}V\right]\mathrm{d}V,\end{aligned} \tag{23}$$

or

$$\begin{aligned}&\frac{1}{\rho_{\mathrm{g}}}\left[\frac{\partial\alpha\rho_{\mathrm{g}}}{\partial t} + \nabla\cdot(\alpha\rho_{\mathrm{g}}\boldsymbol{v}_{\mathrm{g}}) - \Gamma_{\mathrm{g}}\right]\\ &\quad = \int_{V_{\min}}^{V_{\max}}\sum_j S_j V\,\mathrm{d}V.\end{aligned} \tag{24}$$

Here, note that the LHS of Eq. (24) corresponds to the continuity equation of gas phase, and the right-hand side identically equals to zero. Thus, the void fraction transport equation results in the following identities:

$$\begin{aligned}&\frac{\partial\alpha\rho_{\mathrm{g}}}{\partial t} + \nabla\cdot(\alpha\rho_{\mathrm{g}}\boldsymbol{v}_{\mathrm{g}}) - \Gamma_{\mathrm{g}} = 0;\\ &\quad \text{gas-phase mass conservation, and}\end{aligned} \tag{25}$$

$$\begin{aligned}&\int_{V_{\min}}^{V_{\max}}\sum_j S_j V\,\mathrm{d}V = 0;\\ &\quad \text{volume conservation in bubble coalescence}\\ &\quad \text{or break-up.}\end{aligned} \tag{26}$$

2.3. Interfacial area concentration transport equation

The transport equation for the interfacial area concentration is obtained by multiplying Eq. (11) by the average interfacial area of particles $A_{\mathrm{i}}(V)$, with volume V, which is independent of the coordinate system. Integrating the result over the volume of all particles, we obtain

$$\begin{aligned}&\frac{\partial a_{\mathrm{i}}}{\partial t} + \nabla\cdot(a_{\mathrm{i}}\boldsymbol{v}_{\mathrm{i}}) - \left(\frac{\dot{V}}{V}\right)\int_{V_{\min}}^{V_{\max}} fV\,\mathrm{d}A_{\mathrm{i}}\\ &\quad = \int_{V_{\min}}^{V_{\max}}\left[\sum_j S_j + S_{\mathrm{ph}}\right]A_{\mathrm{i}}\,\mathrm{d}V,\end{aligned} \tag{27}$$

where

$$a_{\mathrm{i}}(\boldsymbol{x},t) = \int_{V_{\min}}^{V_{\max}} f(V,\boldsymbol{x},t)A_{\mathrm{i}}(V)\,\mathrm{d}V \tag{28}$$

and

$$\boldsymbol{v}_{\mathrm{i}}(\boldsymbol{x},t) \equiv \frac{\int_{V_{\min}}^{V_{\max}} f(V,\boldsymbol{x},t)A_{\mathrm{i}}(V)\boldsymbol{v}(V,\boldsymbol{x},t)\,\mathrm{d}V}{\int_{V_{\min}}^{V_{\max}} f(V,\boldsymbol{x},t)A_{\mathrm{i}}(V)\,\mathrm{d}V}. \tag{29}$$

Here, $a_{\mathrm{i}}(\boldsymbol{x},t)$ and $\boldsymbol{v}_{\mathrm{i}}(\boldsymbol{x},t)$ are the average interfacial area concentration of all fluid particles of volumes between $V_{\min}$ and $V_{\max}$ and the interfacial velocity, respectively.

By defining the volume and surface area equivalent diameters of fluid particle of volume V as

$$V \equiv \frac{\pi}{6}D_{\mathrm{e}}^3 \tag{30}$$

and

$$A_{\mathrm{i}} \equiv \pi D_{\mathrm{s}}^2, \tag{31}$$

respectively, and combining them with Eq. (27), yields

$$\begin{aligned}&\frac{\partial a_{\mathrm{i}}}{\partial t} + \nabla\cdot(a_{\mathrm{i}}\boldsymbol{v}_{\mathrm{i}}) - \frac{2}{3}\left(\frac{\dot{V}}{V}\right)a_{\mathrm{i}}\\ &\quad = \int_{V_{\min}}^{V_{\max}}\left[\sum_j S_j + S_{\mathrm{ph}}\right]A_{\mathrm{i}}\,\mathrm{d}V.\end{aligned} \tag{32}$$

Therefore, recalling Eq. (22), the interfacial area transport equation is given by

$$\begin{aligned}\frac{\partial a_{\mathrm{i}}}{\partial t} + \nabla\cdot(a_{\mathrm{i}}\boldsymbol{v}_{\mathrm{i}}) &= \frac{2}{3}\left(\frac{a_{\mathrm{i}}}{\alpha}\right)\left(\frac{\partial\alpha}{\partial t} + \nabla\cdot\alpha\boldsymbol{v}_{\mathrm{g}} - \eta_{\mathrm{ph}}\right)\\ &\quad + \int_{V_{\min}}^{V_{\max}}\left[\sum_j S_j + S_{\mathrm{ph}}\right]A_{\mathrm{i}}\,\mathrm{d}V,\end{aligned} \tag{33}$$

where the right-hand side of the equation represents the source and sink due to the change of particle volume,

and those due to the particle interactions and phase change, respectively.

As can be seen in Eq. (33), however, the source/sink terms must be specified with constitutive relations. Therefore, let the particle number source and sink terms and the a_i source and sink terms be denoted, respectively, as

$$\int_{V_{min}}^{V_{max}} \sum_j S_j \, dV = \sum_j R_j \tag{34}$$

and

$$\int_{V_{min}}^{V_{max}} \sum_j S_j A_i \, dV = \sum_j \phi_j. \tag{35}$$

Since ϕ_j can be written in terms of the change of surface area of the fluid particle after the given particle interaction process, it can be expressed as

$$\phi_j = R_j \Delta A_i. \tag{36}$$

Here, ΔA_i is the magnitude of the change in surface area and should account for the given bubble interaction mechanism; i.e., whether it is a break-up process or a coalescence process.

In view of specifying the ΔA_i, we may consider the coalescence and break-up processes as illustrated in Fig. 1. Since the total volume of the particles should be conserved, assigning the subscripts 1 and 2 for the bubbles of small and large volumes, respectively, we have

$$2V_1 = V_2 \quad \text{or} \quad D_2 = 2^{1/3} D_1, \tag{37}$$

such that the change of surface area after a coalescence or a break-up process is given, respectively, by

$$\Delta A_i = -0.413 A_i \quad \text{for a coalescence process and} \tag{38}$$

$$\Delta A_i = 0.260 A_i \quad \text{for a break-up process,} \tag{39}$$

where A_i is the (total amount of) initial surface area of the particle(s) subject to the given particle interaction, and the minus sign accounts for the reduction of surface area compared to the initial surface area. Here, the negative sign in Eq. (38) accounts for the reduction in the bubble surface area after the given interaction process.

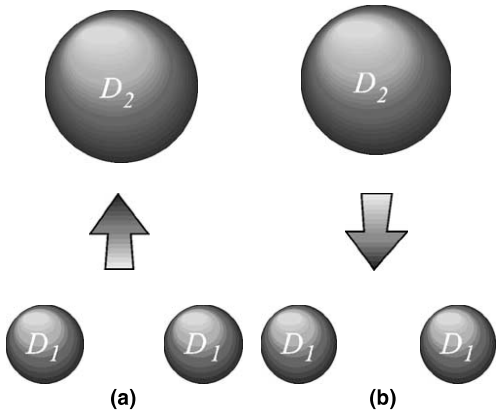

Fig. 1. Illustration of the (a) bubble coalescence and (b) disintegration processes.

Furthermore, since the particle number density can be specified through a_i and α by

$$a_i = nA_i \quad \text{and} \quad \alpha = nV, \tag{40}$$

the particle number density can be written as

$$n = \psi \frac{a_i^3}{\alpha^2} \tag{41}$$

with

$$\psi = \frac{1}{36\pi} \left(\frac{D_{sm}}{D_e} \right)^3, \tag{42}$$

where the Sauter mean diameter is defined by

$$D_{sm} = \frac{6\alpha}{a_i}. \tag{43}$$

Therefore, ϕ_j is given by

$$\phi_j = \frac{1}{3\psi} \left(\frac{\alpha}{a_i} \right)^2 R_j, \tag{44}$$

and similarly, the nucleation source ϕ_{ph}, can be given by

$$\phi_{ph} = \pi D_{bc}^2 R_{ph}, \tag{45}$$

where D_{bc} is the critical bubble size, which should be determined depending on the given nucleation process, namely, critical cavity size for the bulk boiling or condensation process, and bubble departure size for the wall nucleation. The R_{ph} should be modeled independently based on the given phase-changing mechanism, such as nucleation or condensation. Thus, combining with the constitutive relations given above, we can rewrite the interfacial area transport equation as

$$\frac{\partial a_i}{\partial t} + \nabla \cdot (a_i \boldsymbol{v}_i) = \frac{2}{3} \left(\frac{a_i}{\alpha} \right) \left(\frac{\partial \alpha}{\partial t} + \nabla \cdot \alpha \boldsymbol{v}_g - \eta_{ph} \right) + \frac{1}{3\psi} \left(\frac{\alpha}{a_i} \right)^2 \sum_j R_j + \pi D_{bc} R_{ph}. \tag{46}$$

2.4. One-group interfacial area transport equation

In view of small bubble transport, where all the bubbles are approximated as spherical in shape, the bubble Sauter mean diameter is approximately equal to the volume equivalent diameter. Therefore, ψ defined in Eq. (42) reduces to

$$\psi = \frac{1}{36\pi} = 8.85 \times 10^{-3} \tag{47}$$

and the nucleation source, η_{ph}, can be written as

$$\eta_{ph} \equiv \int_{V_{min}}^{V_{max}} S_{ph} V \, dV \approx R_{ph} \frac{\pi}{6} D_{bc}^3. \tag{48}$$

Furthermore, noting that the critical bubble size due to the nucleation is much smaller than the bubble Sauter mean diameter, the following simplification can be made

$$\left(\frac{D_{bc}}{D_{sm}}\right) \approx 0. \tag{49}$$

Therefore, the interfacial area transport equation for dispersed bubbles (or one-group interfacial area transport equation) can be reduced further from Eq. (46) to

$$\frac{\partial a_i}{\partial t} + \nabla \cdot (a_i \boldsymbol{v}_i) \approx \frac{2}{3}\left(\frac{a_i}{\alpha}\right)\left(\frac{\partial \alpha}{\partial t} + \nabla \cdot \alpha \boldsymbol{v}_g\right) + \frac{1}{3\psi}\left(\frac{\alpha}{a_i}\right)^2 \sum_j R_j + \pi D_{bc}^2 R_{ph}. \tag{50}$$

Here, the *one-group* is to note the fact that, in this regime, the transport phenomena of all the dispersed fluid particles are similar in view of drag and interaction mechanisms. In order to account for the various sizes of bubbles, such as cap or Taylor bubbles, a *two-group* approach should be sought as will be discussed later in Section 4 of the present study.

As shown in Eq. (50), the right-hand side of the equation is constituted with source/sink terms that must be specified by the constitutive relations. In view of this, the major fluid particle interaction mechanisms were identified and mechanistic models of the three major mechanisms that occur in bubbly flow conditions have been established [8,10,11]. In bubbly flow conditions, they include:

- Disintegration due to the impact of turbulent eddies (TI),
- Coalescence through random collision driven by turbulent eddies (RC), and
- Coalescence due to the acceleration of the following bubble in the wake of the preceding bubble (WE).

The schematic illustrations of these mechanisms are shown in Fig. 2. Final expressions for the particle number source or sink terms due to such mechanisms are given by [10,11]

$$R_{TI} = C_{TI}\left(\frac{nu_t}{D_b}\right)\exp\left(-\frac{We_{cr}}{We}\right)\sqrt{1-\frac{We_{cr}}{We}},$$
where $We > We_{cr}$: TI(Source), (51)

$$R_{RC} = C_{RC}\left[\frac{n^2 u_t D_b^2}{\alpha_{max}^{1/3}\left(\alpha_{max}^{1/3} - \alpha^{1/3}\right)}\right] \times \left[1 - \exp\left(-C\frac{\alpha_{max}^{1/3}\alpha^{1/3}}{\alpha_{max}^{1/3} - \alpha^{1/3}}\right)\right]: \text{RC(Sink)} \tag{52}$$

and

$$R_{WE} = C_{WE} C_D^{1/3}(D_b) n^2 D_b^2 u_r(D_b): \text{WE(Sink)}. \tag{53}$$

Here, D_b, We_{cr}, α_{max}, and C_D are the bubble diameter, critical Weber number over which the bubble break-up occurs, maximum packing limit, and drag coefficient, respectively, and C_{TI}, C_{RC}, C and C_{WE} are the coefficients to be determined through experiment. In the scope of the present study, detailed modeling processes are omitted, and the readers are asked to refer to the previous studies by Wu et al. [10] and Kim [11].

3. Model evaluation

3.1. One-dimensional steady state one-group interfacial area transport equation

In order to formulate the interfacial area transport equation so that it applies to the conditions of various two-phase flow regimes, the model must account for various types of bubbles varying in both size and shape. These bubble types depend on both the flow conditions and the geometry of the flow duct. In most two-phase flow conditions, these include; spherical, distorted, cap, Taylor and churn-turbulent bubbles. The differences in shape and size of such bubbles cause substantial differences in their transport mechanisms due to the differences

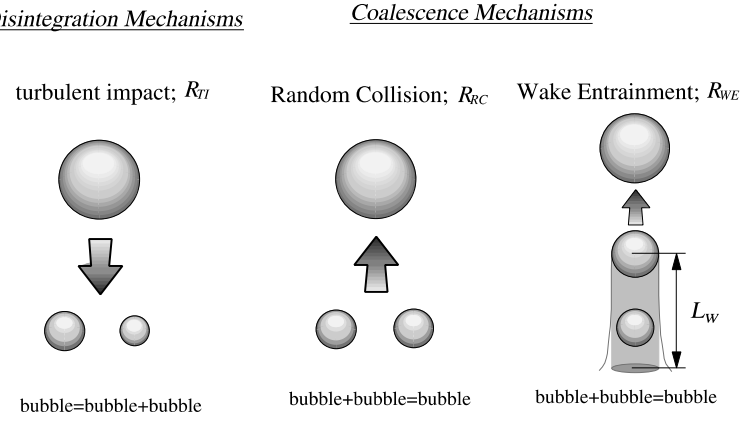

Fig. 2. Major bubble interaction mechanisms in bubbly flow (group 1) conditions.

in drag forces. Hence, in view of different transport characteristics, the bubbles can be categorized into two groups, namely; group 1 for spherical and distorted bubbles and group 2 for cap, Taylor and churn-turbulent bubbles. Thus, two sets of interfacial area transport equation should be formulated in order to describe particle transport phenomena over the wide range of two-phase flow conditions. In the present study, however, the experimental database on group 2 bubble transport is yet to be sufficient. Therefore, the focus is only on the one-group interfacial area transport equation for bubbly flow and the model evaluation is performed using the available database for bubbly flow conditions.

The one-group interfacial area transport equation can be obtained by combining Eq. (50) with the source and sinks terms given by Eqs. (51)–(53). In the present evaluation study, the equation and the local experimental data are spatially averaged over the tube cross-sectional area to simplify the evaluation process. This process assumes all parameters exhibit nearly uniform profiles along the radial direction, which was found to be consistent with the experimental data in most flow conditions. Hence, the covariance terms in the averaging process are neglected. This assumption was found to be consistent with the data. Also, accounting for the fact that the experiments were performed under adiabatic air/water two-phase conditions, the nucleation source term, R_{ph}, was omitted from the model. Furthermore, noting from the experimental data that the bubble size across the flow duct at a given axial level was nearly uniform in bubbly flow conditions, the a_i weighted bubble interfacial velocity was approximated as

$$\langle\langle v_i\rangle\rangle \equiv \frac{\langle a_i v_i\rangle}{\langle a_i\rangle} \approx \frac{\langle \alpha v_g\rangle}{\langle\alpha\rangle} = \langle\langle v_g\rangle\rangle. \tag{54}$$

Hence, assuming that there is no radial dependence in fluid properties and the ideal gas law is valid, the steady-state one-dimensional one-group interfacial area transport equation for adiabatic bubbly flow can be obtained as

$$\begin{aligned}
&\frac{\partial}{\partial z}\left(\langle a_i\rangle\langle\langle v_g\rangle\rangle\right) \\
&\quad = \left(\frac{2\langle a_i\rangle\langle\langle v_g\rangle\rangle}{3p}\right)\left(-\frac{\partial p}{\partial z}\right) + C_{TI}\frac{1}{18}\left(\frac{\langle a_i\rangle^2}{\langle\alpha\rangle}\langle u_t\rangle\right) \\
&\qquad \times \sqrt{1-\frac{We_{cr}}{We}}\exp\left(-\frac{We_{cr}}{We}\right) - C_{RC}\frac{1}{3\pi} \\
&\qquad \times \frac{\langle a_i\rangle^2\langle u_t\rangle}{\langle\alpha\rangle_{max}^{1/3}\left(\langle\alpha\rangle_{max}^{1/3} - \langle\alpha\rangle^{1/3}\right)} \\
&\qquad \times \left[1-\exp\left(-C\frac{\langle\alpha\rangle_{max}^{1/3}\langle\alpha\rangle^{1/3}}{\langle\alpha\rangle_{max}^{1/3} - \langle\alpha\rangle^{1/3}}\right)\right] \\
&\qquad - C_{WE}C_D^{1/3}\frac{1}{3\pi}\langle a_i\rangle^2\langle u_r\rangle.
\end{aligned} \tag{55}$$

where the left-hand side of the equation represents the change of interfacial area concentration along the axial direction, and the right-hand side is composed of source due to bubble expansion by pressure drop (XP), source due to turbulent impact bubble break-up (TI), sink due to bubble coalescence through random collision induced by turbulent eddies (RC) and sink due to coalescence in the wake region of the preceding bubble (WE), respectively.

3.2. Experimental conditions

In the present study, the model is evaluated with the experimental data acquired within the bubbly flow conditions in various sizes of round tubes. The adiabatic air–water vertical co-current loop is constructed from round acrylic tubes of three different sizes as shown in Fig. 3. The two-phase mixture is generated by injecting air into the test section through a sparger. In the present design, the bubble size at the inlet of the test section is controlled by fixing the liquid flow rate (j_{f1}) that shears the bubbles off from the sparger. The total liquid flow rate is then controlled by varying the main liquid line (j_{f2}). This mechanism allows the inlet bubble size to be uniform, such that the bubble size at the inlet is controlled to be approximately 1–2 mm in diameter.

The detailed local time-averaged two-phase flow parameters are acquired using the state-of-the-art miniaturized double-sensor conductivity probe at three different axial levels. At each level, the probe is traversed along the radial direction at a constant increment. The increment is varied depending on the measurement location and the tube size. The finest control possible is an increment of 1.27 mm. In acquiring the local data, thousands of bubbles were sampled at one local point, such that the measurement error associated with the conductivity probe can be minimized within ±10% [12, 13]. The experimental conditions and the flow conditions presented in the paper are summarized in Fig. 4, where the solid line in the figure represents the boundary between the bubbly and the slug flow regimes suggested by Mishima and Ishii [14].

In order to evaluate the model with experimental data, the adjustable coefficients in the model must be specified. In the present study, the coefficients are determined using the given experimental conditions, such as liquid superficial velocity, gas superficial velocity, and void fraction. For example, in highly turbulent flow conditions, the turbulent break-up (TI) and the random collision (RC) coalescence mechanisms are assumed to be dominant, whereas in low liquid flow with high void fraction, the dominant mechanism is assumed to be the wake-entrainment (WE). Furthermore, the constant C in the RC, which accounts for the effective range of influence of turbulent eddies in driving bubbles to collisions,

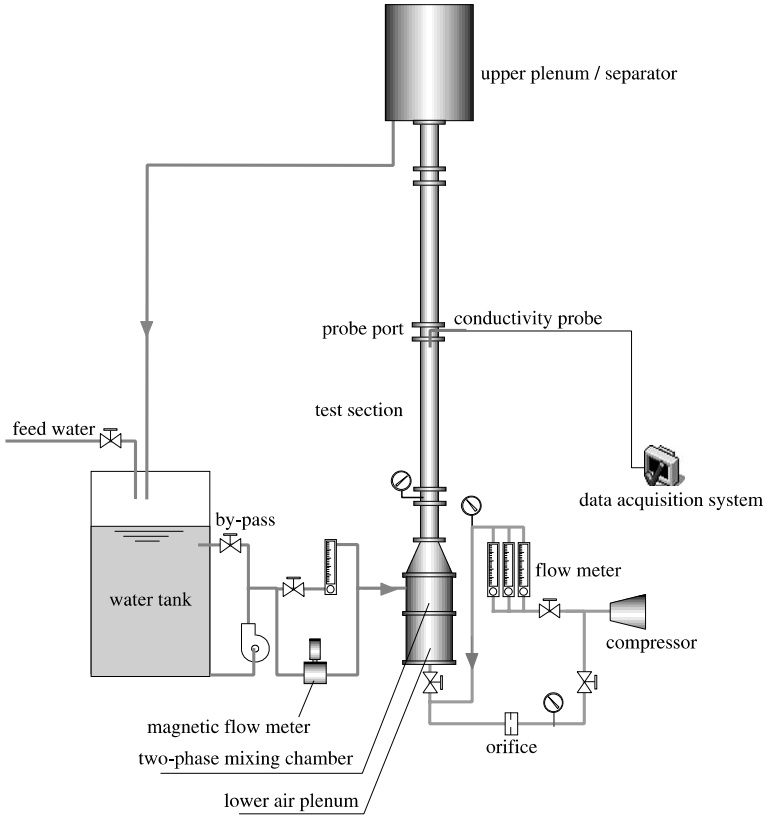

Fig. 3. Schematic diagram of the experimental loop.

is assumed to be 3.0. In estimating the critical Weber number, the value was varied from 2.3 to 8.0, based on the previous studies [15,16]. The value, which yields the best results for all of the current flow conditions, was then chosen. The final values for the coefficients were determined to be

Wake entrainment: $C_{WE} = 0.002$;

Random collision: $C_{RC} = 0.004$; $C = 3.0$; $\alpha_{max} = 0.75$;

Turbulent impact: $C_{TI} = 0.085$; $We_{cr} = 6.0$.

Here, the maximum packing limit is based on the hexagonal-closed-packed bubble distribution, assumed in modeling the RC mechanism [10].

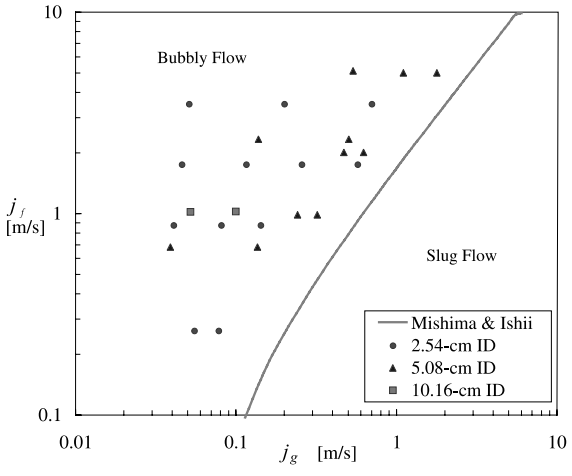

Fig. 4. The experimental flow conditions. The flow regime transition line is given by Mishima and Ishii [14].

3.3. Evaluation results

The results of the model evaluation for all of the present experimental conditions are shown in Fig. 5. In the figure, the axial development of interfacial area predicted by the model and the experimental data are plotted for each flow condition. The solid lines and the symbols depict the model predictions and the experimental data, respectively. So as not to hamper the clarity of Fig. 5(a) and (b), the experimental error is only depicted in Fig. 5(c). However, for all runs the error is estimated to be $\pm 10\%$.

As shown in Fig. 5, overall agreement between the model and the data is within the measurement error of

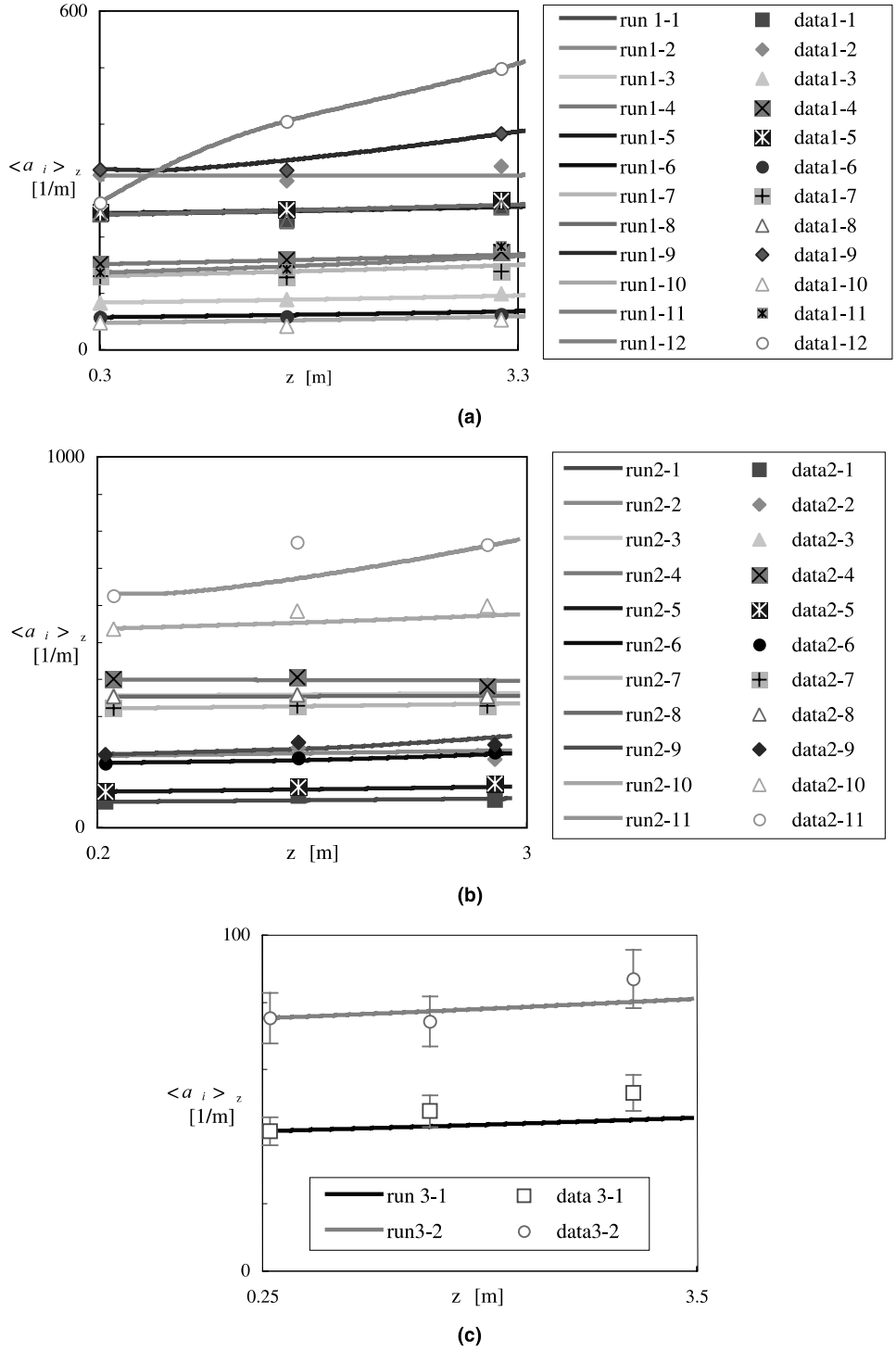

Fig. 5. Evaluation of the model with experimental data. (a) Data obtained in 2.54 cm ID pipe. (b) Data obtained in 5.08 cm ID pipe. (c) Data obtained in 10.16 cm ID pipe (error bar ±10%).

approximately ±10%. Most disagreement was observed in conditions approaching the transition to slug flow, such as Runs 2-10 and 2-11. In these runs, occasional cap bubbles were noted. Therefore, the discrepancy most

likely stems from the fact that the one-group model does not account for transport behavior of the cap bubble group, suggesting that a two-group formulation is necessary to adequately predict the transition to slug flow.

The deviation from the model prediction is most significant in the data obtained in the 10.16 cm ID pipe as shown in Fig. 5(c). However, in the large diameter pipe, the bubbles had a larger component of velocity in the transverse direction and some local re-circulation patterns were also observed. Such re-circulation phenomenon was most severe near the exit of the test section, where the flow was diverted into a horizontal section before the accumulating tank. These flow patterns are not accounted for either in the one-dimensional model or in the local probe application. Hence, it is believed that such shortcomings limit the accuracy in both model prediction and the experimental data. A more extensive database for the large diameter pipe flows is needed for sensible analysis on the model. Nevertheless, the overall agreement between the model predictions and the data taken in various sizes of pipes are quite acceptable.

Fig. 6(a) and (b) depict the contributions from individual source and sink mechanisms to the total change in a_i in the 2.54 and 5.08 cm ID pipes, respectively. In both runs, bubble expansion due to the pressure gradient along the pipe (XP) and the RC mechanism dominate the overall change in a_i. Furthermore, for these conditions the interactions due to WE is found to be relatively weak, whereas the TI source term begins to have some effect in Run 2-6 at axial levels greater than 1.4 m.

4. Framework of the two-group interfacial area transport equation

Section 3 alluded to the fact that in order to model the interfacial transport phenomena of fluid particles in all two-phase flow regimes, the effects due to the differences in bubble size and shape should be carefully considered. These include more mechanistic modeling efforts on additional bubble interaction mechanisms and considerations on interactions between the bubbles of different shapes and sizes. Therefore, two transport equations for two different groups of bubbles should be sought. The group 1 transport equation describes the transport phenomena of small-dispersed and distorted bubbles, whereas the group 2 transport equation describes the transport phenomena of cap/slug/churn-turbulent bubbles.

The theoretical approach in developing the two-group particle number transport equation can be established by defining the critical bubble volume by which the bubble group is determined, such that

$$\frac{\partial n_1}{\partial t} + \nabla \cdot (n_1 \boldsymbol{v}_{\mathrm{pm}_1}) = -f_c V_c \left(\frac{\dot{V}}{V} \right) + \sum_j R_{j1} + R_{\mathrm{ph}_1}: \quad \text{Group 1;} \tag{56}$$

$$\frac{\partial n_2}{\partial t} + \nabla \cdot (n_2 \boldsymbol{v}_{\mathrm{pm}_2}) = f_c V_c \left(\frac{\dot{V}}{V} \right) + \sum_j R_{j2} + R_{\mathrm{ph}_2}: \quad \text{Group 2,} \tag{57}$$

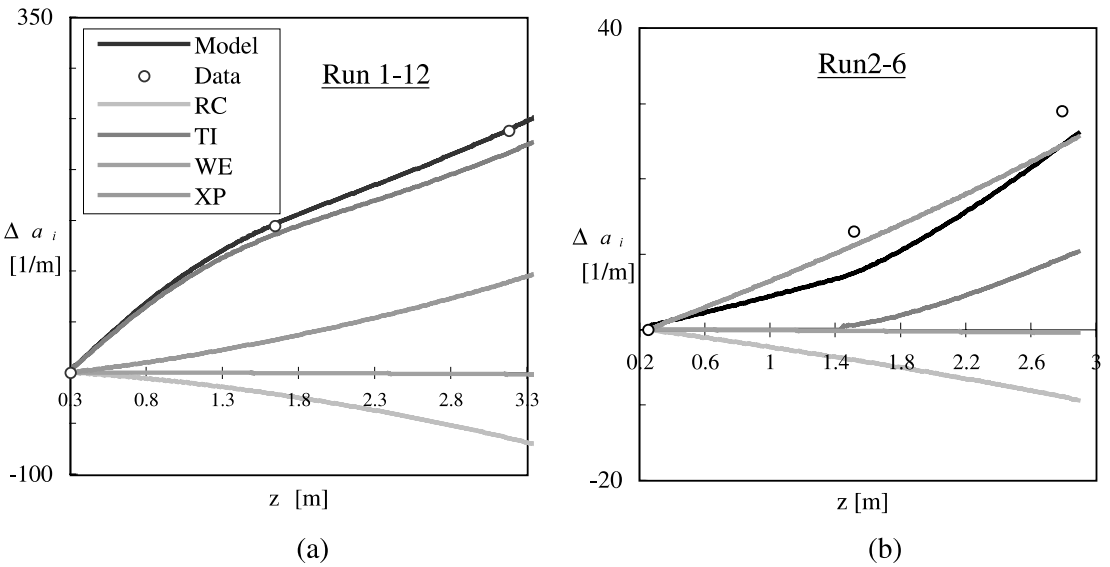

Fig. 6. Contribution of individual bubble interaction mechanisms to total change in a_i. (a) Run 1-12: $j_g = 0.702$ m/s and $j_f = 3.49$ m/s in a round pipe of 2.54 cm ID. (b) Run 2-6: $j_g = 0.506$ m/s and $j_f = 2336$ m/s in a round pipe of 5.08 cm ID.

where V_c is the critical bubble volume defined by the maximum distorted bubble limit given by Ishii and Zuber [17] as

$$D_{\mathrm{dmax}} = 4\sqrt{\frac{\sigma}{g\Delta\rho}}, \tag{58}$$

over which the bubble becomes cap in shape. Hence, the interfacial area transport equation can be readily obtained as

$$\frac{\partial a_{\mathrm{i}1}}{\partial t} + \nabla\cdot(a_{\mathrm{i}1}\boldsymbol{v}_{\mathrm{i}1}) + \int_{V_{\mathrm{min}}}^{V_c}\left[A_{\mathrm{i}}\frac{\partial}{\partial V}\left(f\frac{\mathrm{d}V}{\mathrm{d}t}\right)\right]\mathrm{d}V = \int_{V_{\mathrm{min}}}^{V_c}\left[\sum_j S_j + S_{\mathrm{ph}}\right]A_{\mathrm{i}}\,\mathrm{d}V: \quad \text{Group 1;} \tag{59}$$

$$\frac{\partial a_{\mathrm{i}2}}{\partial t} + \nabla\cdot(a_{\mathrm{i}2}\boldsymbol{v}_{\mathrm{i}2}) + \int_{V_c}^{V_{\mathrm{max}}}\left[A_{\mathrm{i}}\frac{\partial}{\partial V}\left(f\frac{\mathrm{d}V}{\mathrm{d}t}\right)\right]\mathrm{d}V = \int_{V_c}^{V_{\mathrm{max}}}\sum_j S_j A_{\mathrm{i}}\,\mathrm{d}V: \quad \text{Group 2.} \tag{60}$$

Furthermore, the closure relations for the two-group a_{i} transport equation can be given such that

$$\int_{V_{\mathrm{min}}}^{V_{\mathrm{max}}}\sum_j S_j\,\mathrm{d}V = R_j \quad \text{and}$$

$$\int_{V_{\mathrm{min}}}^{V_{\mathrm{max}}}\sum_j A_{\mathrm{i}}S_j\,\mathrm{d}V = \phi_j; \tag{61}$$

$$\phi_j = R_j\Delta A_{\mathrm{i}} \quad \text{and} \quad \phi_{\mathrm{ph}} = R_{\mathrm{ph}}\pi D_{\mathrm{bc}}^2; \tag{62}$$

$$n = \psi\frac{a_{\mathrm{i}}^3}{\alpha^2}, \quad \text{where } \psi = \frac{1}{36\pi}\left(\frac{D_{\mathrm{sm}}}{D_{\mathrm{e}}}\right)^3; \tag{63}$$

$$\alpha = \alpha_1 + \alpha_2; \tag{64}$$

$$a_{ik} = n_k\bar{A}_{ik}; \tag{65}$$

$$\Gamma_{\mathrm{g}} = \Gamma_{\mathrm{g}1} + \Gamma_{\mathrm{g}2}; \tag{66}$$

and

$$\boldsymbol{v}_{\mathrm{g}} = \frac{\alpha_1\boldsymbol{v}_{\mathrm{g}1} + \alpha_2\boldsymbol{v}_{\mathrm{g}2}}{\alpha_1 + \alpha_2}. \tag{67}$$

Here, in solving the two-group transport equation with the closure relations given through Eqs. (61)–(67), the gas-phase continuity equations for group 1 and group 2 bubbles should be employed. In specifying the gas-phase velocities for the two groups of bubbles, however, the drift flux model can be employed in conjunction with the experimental measurements instead of employing the momentum equation.

The major challenge in developing the two-group transport equation arises from the complicated bubble transport phenomena and their interactions. With the introduction of another bubble group, additional source and sink terms specific to the larger bubble group, as well as inter-group interactions must be modeled. For instance, the source terms for the larger bubbles should include the shearing off of small bubbles at the rim of large bubbles (SO) and the break-up due to surface instability (SI). Moreover, some interaction mechanisms will apply to both groups and may require modifications to Eqs. (51)–(53). Since the sink terms of one group may prove to be the source terms of the other, these inter-group mechanisms will have to be developed in concert with both groups, adding to the complexity of the development process. The pictorial representation of the major two-group interaction mechanisms, and the summary of all the intra- and inter-group mechanisms to be considered are presented in Fig. 7 and Table 1, respectively.

5. Summary and conclusions

The two-fluid model considers each phase separately in terms of two sets of conservation equations. Such separate treatment of the two phases and detailed considerations of phase interactions allow the two-fluid model describe the two-phase flow system most accurately among available models. In the two-fluid model, however, since the averaged macroscopic fields of each phase are not independent of each other, interaction terms arise. These interaction terms couple the transport of mass, momentum, and energy of each phase across the interfaces as source terms, expressed as a function of interfacial area concentration, a_{i}, and the driving flux. Currently, static flow regime maps and associated transition criteria are utilized to characterize the interfacial transfer terms. Improving the formulation of these terms represents the best opportunity to enhance the capability of the two-fluid model. To improve the treatment of interfacial structure with an aim of enhancing the two-fluid model, a one-group interfacial area transport equation was developed, which dynamically predicts the axial variations in interfacial area concentration. In conjunction with the theoretical efforts, detailed benchmark experiments were performed for adiabatic air–water bubbly flow in round tubes of three different flow areas. In all of the evaluation studies, the model agreed well with the experimental data within the measurement error of $\pm 10\%$. The characteristic contributions from individual interaction mechanisms in total change of interfacial area concentration are also demonstrated. Also presented are some fundamental considerations in the development of two-group interfacial area transport equation in view of interfacial area transport of various bubbles in wider two-phase flow regimes.

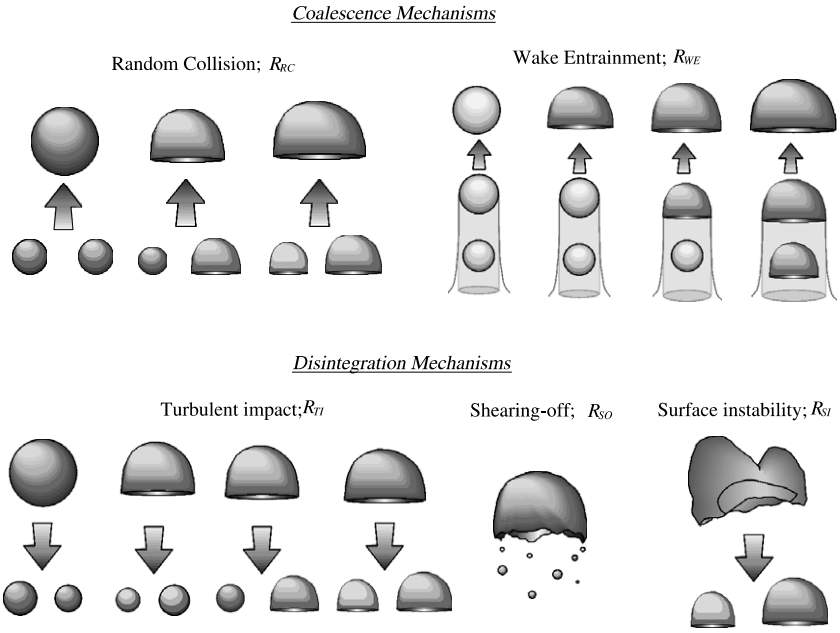

Fig. 7. Schematic illustrations of two-group bubble interaction.

Table 1
Summary of inter- and intra-group interaction mechanisms and their contributions

Notation	Mechanisms	Contribution	Remarks
$R_{TI}^{(1)}$	Turbulent disintegration	$(1) \Rightarrow (1)+(1)$	Source in 1
$R_{TI}^{(2,11)}$	Turbulent disintegration	$(2) \Rightarrow (1)+(1)$	Source in 1 Sink in 2
$R_{TI}^{(2,12)}$	Turbulent disintegration	$(2) \Rightarrow (1)+(2)$	Source in 1 Sink in 2 (No number change)
$R_{TI}^{(2)}$	Turbulent disintegration	$(2) \Rightarrow (2)+(2)$	Source in 2
$R_{RC}^{(1)}$	Random collision	$(1) \Rightarrow (1)$	Sink in 1
$R_{RC}^{(11,2)}$	Random collision	$(1)+(1) \Rightarrow (2)$	Sink in 1 Source in 2
$R_{RC}^{(12,2)}$	Random collision	$(1)+(2) \Rightarrow (2)$	Sink in 1 Source in 2 (No number change)
$R_{RC}^{(2)}$	Random collision	$(2)+(2) \Rightarrow (2)$	Sink in 2
$R_{WE}^{(1)}$	Wake entrainment	$(1) \Rightarrow (1)$	Sink in 1
$R_{WE}^{(11,2)}$	Wake entrainment	$(1)+(1) \Rightarrow (2)$	Sink in 1 Source in 2
$R_{WE}^{(12,2)}$	Wake entrainment	$(1)+(2) \Rightarrow (2)$	Sink in 1 Source in 2 (No number change)
$R_{WE}^{(2)}$	Wake entrainment	$(2)+(2) \Rightarrow (2)$	Sink in 2
$R_{SO}^{(2,1)}$	Shearing-off	$(2) \Rightarrow (2)+N(1)$	Source in 1 (Multiple number) Sink in 2 (No number change)
$R_{SI}^{(2)}$	Surface instability	$(2) \Rightarrow (2)+(2)$	Source in 2

In the notation column, the superscripts in the parenthesis represent the group numbers of the interacting and the resulting bubbles, respectively. Single superscript implies that the interaction is within the given group, i.e., intra-group interaction.

Acknowledgements

This study was supported by the US NRC Office of Nuclear Regulatory Research.

References

[1] P. Vernier, J.M. Delhaye, General two-phase flow equations applied to the thermohydrodynamics of boiling nuclear reactor, Energ. Primaire 1 (1968) 5.
[2] M. Ishii, Thermo-fluid dynamic theory of two-phase flow, Collection de la Direction des Etudes et Recherches d'Electricite de France, Eyrolles, Paris, 1975.
[3] J.A. Boure, Mathematical modeling of two-phase flows, in: S. Banerjee, K.R. Weaver (Eds.), Proceedings of the CSNI Specialist Meeting, August 3–4, Toronto, Canada, A.E.C.L., vol. 1, 1978, p. 85.
[4] M. Ishii, K. Mishima, Study of two-fluid model and interfacial area, Argonne National Laboratory Report, ANL-80-111, 1980.
[5] M. Ishii, K. Mishima, Two-fluid model and hydrodynamic constitutive relations, Nucl. Eng. Des. 82 (1984) 107–126.
[6] G.A. Mortensen, Long-term plan for NRC thermal-hydraulic code development, Report to USNRC under contract DE-AC07-94ID13223, March 1995.
[7] J.M. Kelly, Thermal-hydraulic modeling needs for passive reactors, OECD/CSNI Specialist Meeting on Advanced Instrumentation and Measurement Techniques, Santa Barbara, CA, USA, March 17–20, 1997.
[8] G. Kocamustafaogullari, M. Ishii, Foundation of the interfacial area transport equation and its closure relations, Int. J. Heat Mass Transfer 38 (3) (1995) 481–493.
[9] J.N. Reyes, Statistically derived conservation equations for fluid particle flows, in: Fifth Proceedings of the ANS-THD, 1989 ANS Winter Meeting, San Francisco, CA, November, 1989, p. 12.
[10] Q. Wu, S. Kim, M. Ishii, S.G. Beus, One-group interfacial area transport in vertical bubbly flow, Int. J. Heat Mass Transfer 41 (8/9) (1998) 1103–1112.
[11] S. Kim, Interfacial area transport equation and measurement of local interfacial characteristics, Ph.D. Thesis, School of Nuclear Engineering, Purdue University, November 1999.
[12] Q. Wu, S. Kim, D. McCreary, M. Ishii, S.G. Beus, Measurement of interfacial area concentration in two-phase bubbly flow, in: 1997 ANS Winter Meeting, Albuquerque, NM, November 10–20, TANSAO 77, 1997, p. 437.
[13] Q. Wu, M. Ishii, Sensitivity study on double-sensor conductivity probe for the measurement of interfacial area concentration in bubbly flow, Int. J. Multiphase Flow 25 (1) (1999) 155–173.
[14] K. Mishima, M. Ishii, Flow regime transition criteria for upward two-phase flow in vertical tubes, Int. J. Heat Mass Transfer 27 (5) (1984) 723–737.
[15] M. Ishii, T.C. Chawla, Local drag laws in dispersed two-phase flow, Argonne National Laboratory Report, ANL-79-105, NUREG/CR-1230, 1979.
[16] M.J. Prince, H.W. Blanch, Bubble coalescence and break-up in air-sparged bubble columns, AIChE J. 36 (10) (1990) 1485–1499.
[17] M. Ishii, N. Zuber, Drag coefficient and relative velocity in bubbly, droplet or particulate flows, AIChE J. 25 (1979) 843.